CHALMERS
UNIVERSITY OF TECHNOLOGY

Explicit Finite Element Modeling of Hood Closing in LS-Dyna

Master's thesis in Applied Mechanics
Volvo Cars report no. 91520-2016-078

PETER LAGERVALL
MATTIAS RUNDQWIST

Department of Applied Mechanics
CHALMERS UNIVERSITY OF TECHNOLOGY
Gothenburg, Sweden 2016

Master's thesis 2016:48

Explicit Finite Element Modeling of Hood Closing in LS-Dyna

PETER LAGERVALL
MATTIAS RUNDQWIST

Department of Applied Mechanics
Division of Material and Computational Mechanics
Chalmers University of Technology
Gothenburg, Sweden 2016

Explicit Finite Element Modeling of Hood Closing in LS-Dyna

PETER LAGERVALL
MATTIAS RUNDQWIST

Master's thesis 2016:48
Department of Applied Mechanics
Division of Material and Computational Mechanics
Chalmers University of Technology
SE-412 96 Gothenburg
Telephone +46 31 772 1000

Cover: Finite element model of a Volvo XC90 front, with the hood highlighted in red.

Printed by Volvo Car Corporation
Gothenburg, Sweden 2016

Explicit Finite Element Modeling of Hood Closing in LS-Dyna
PETER LAGERVALL
MATTIAS RUNDQWIST
Department of Applied Mechanics
Chalmers University of Technology

Abstract

A model of a car front end is set up in LS-Dyna to analyze the displacements of the hood and its contacts to the surrounding components during slam closing. The Volvo XC90 is used as a case study. In the current Volvo Cars slam analysis method an implicit Nastran solver is used. The complex nature of this load case, with nonlinearities and large displacements, suggests that using an explicit solver may be more efficient. The rubber components, i.e. the seal and the bump stops, are modeled with the hyperelastic Yeoh model. Airbag modeling is used to pressurize the seal cavity. The locking mechanism, with the real geometries of the lock parts kept, is included in the model.

The hood displacement at four positions along the edge of the hood during the slam event is compared to physical test data and to results from the current Volvo modeling method. Results show that the proposed model is conservative in most cases, overpredicting the displacement at three out of four observed points. Compared to the current Volvo Cars hood slam model, the proposed model is closer to test data in three out of four cases. Further, the simulation time is reduced with the LS-Dyna model by 40 - 50%.

Contacts are more convenient to set up in the LS-Dyna model and the contact forces are easily obtained from the results. The modeling method that is developed gives displacements that can be clearly visualized. It will be easier to judge the risk of damaging contacts between the parts with the new modeling method compared to the current method. Further, efficiency can be increased when models can be more easily shared between CAE durability and CAE safety.

The modeling method is verified by implementing it in a Volvo S90 model and performing an overslam analysis. The analysis shows sufficiently well correlated results, suggesting that the model is robust and applicable not only to the XC90 model, but also to other car models.

Keywords: Explicit FE-modeling, hood slam, LS-Dyna, hyperelasticity, Yeoh model, vented sealing, airbag

Preface

This thesis is the result of our last semester at the Master's program in Applied Mechanics at Chalmers University of Technology. The work was performed during the spring 2016 at the CAE Durability Body and Trim department of Volvo Cars and supervised by M.Sc. Wasim Asgher, M.Sc. Kristofer Engelbrektsson and Ph.D. Åsa Sällström. Professor Magnus Ekh at the division of Material and Computational Mechanics at Chalmers University of Technology has been the examiner.

First of all we would like to thank our supervisors for their dedication and guidance throughout the project. We would also like to thank professor Magnus Ekh, for support and expert advising along the way.

A special thanks goes to Kai Kallio and Emil Nilsson at the Material Center for Mechanical Testing at Volvo Cars, for tips and help regarding material testing and for field expertise and monitoring throughout the component testing process. Further thanks to Thomas Johansson and Siv Karlsson at Gislaved Gummi for sharing material test data and providing other useful material information.

Claes Ljunqvist at the CAE safety department of Volvo Cars and Jimmy Forsberg of Dynamore Nordic have provided many useful discussions on airbag theory and contributed with hands-on airbag modeling know-how. We are truly grateful to them.

Last but not least, we would like to thank manager Annika Lundberg and everybody at CAE Durability Body and Trim department at Volvo Cars for providing a creative, open and friendly work environment.

Peter Lagervall & Mattias Rundqwist,
Gothenburg June 2016

Contents

1 Introduction **1**
1.1 Objectives . . . 1
1.2 Thesis outline . . . 2

2 Hood overslam **5**
2.1 Event and key component identification . . . 5
2.2 XC90 model for hood overslam analysis . . . 6
2.3 Current hood overslam analysis method . . . 6

3 Bump stops **7**
3.1 Material model . . . 7
3.1.1 Parameter identification from material test . . . 8
3.1.2 Bump stop and fender carrier compression test . . . 8
3.1.3 Correlation and parameter tuning . . . 9
3.2 Contact modeling in LS-Dyna . . . 10

4 Hood sealing **11**
4.1 Material model . . . 11
4.2 Seal cavity . . . 12

5 Locking mechanism **15**

6 Complete model **17**
6.1 Loads and boundary conditions . . . 17
6.2 Unknown parameters . . . 17

7 Output from complete model **21**
7.1 Hood overtravel . . . 21
7.2 Hood-to-lamp contact force . . . 23
7.3 Bump stop and hood seal forces . . . 23
7.4 Hood velocity components . . . 24
7.5 Computing power performance . . . 25

8 S90 model **27**

9 Discussion **29**
9.1 Model and results . . . 29
9.2 Material model . . . 29
9.3 Seal cavity and airbag modeling . . . 30

10 Future work **31**

11 Concluding remarks **33**

A Rubber elasticity **I**
A.1 Kinematics: Deformation tensors I
A.2 The Yeoh model II
A.3 Tension and compression tests III
A.4 Fit to test data IV

1 Introduction

In the automotive industry the lead time to develop new cars is constantly reduced. Also, with the new car designs, smaller and smaller gaps around the hood is desired. Therefore fast and accurate CAE methods to simulate the closing of a hood is needed to ensure that the hood does not impact the surrounding components too severely.

It is common to model static loading with relatively small deformations implicitly. More complex dynamic load cases combined with nonlinearities and larger deformations, as in crash applications or other impact events, are computationally more intensive. To save computational power in such cases, an explicit integration scheme may be applied.

In the current modeling method for hood slam analysis at Volvo Cars, contacts are generally not modeled. However in a hood slam event, there is a significant contact area between the hood and its neighboring parts. For a more thorough analysis, it is of importance to model these contacts properly. The finite element solver software LS-Dyna is commonly used in crash analysis and is well developed for explicit modeling and contact formulation.

The requirements on a hood may be contradictory since it should ideally be stiff for solidity and durability purposes, but weak in the right areas for crashworthiness and pedestrian safety. Making the crash modeling method and the durability stiffness modeling methods more compatible would ease the optimization process when designing a new car.

What is more, the total delivery time may be significantly reduced if LS-Dyna would be applied, since pre-existing crash models are likely to be available and ready to be modified for slam analysis. Merging the methodologies of different departments within the organization would allow not only for time and monetary savings but ultimately also for a more accessible and efficient development environment.

1.1 Objectives

A modeling method for simulating hood slam in LS-Dyna is to be established. The method should enable increased efficiency and shorter total delivery time than the current Volvo method.

Detailed investigations of the nonlinear and dynamic properties of the bump stops, seal and locking mechanism should be performed. This should give a deeper knowledge of the required modeling of the components. To account for the impact between the hood and the rest of the front body, contact formulations are to be implemented in the finite element model.

Starting with a full front finite element model from the safety department at Volvo Cars, accurate results for overslam analysis should be enabled without making too extensive or time consuming changes in the finite element model. To as great extent as possible, the real geometries of components are to be kept.

1.2 Thesis outline

The components of particular interest in the closing analysis are identified. The modeling of these components are studied in detail. A Volvo XC90 is used as a case study in an explicit LS-Dyna solver. The results from the new LS-Dyna model is compared to the current Nastran model used at Volvo Cars and to test data. Finally, to investigate its robustness, the method is implemented in a Volvo S90 model. The methodology of the work in the thesis is outlined in Figure 1.1.

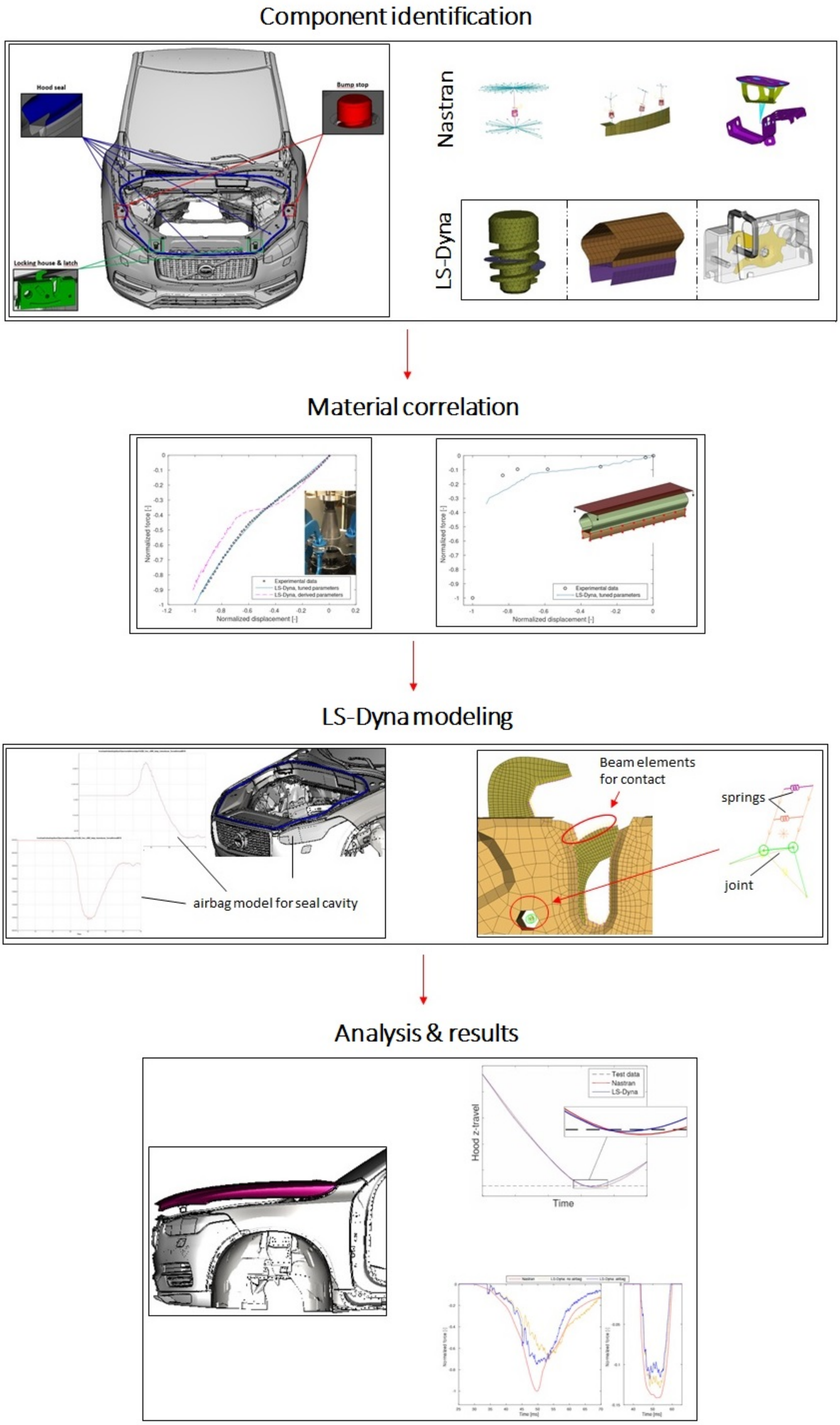

Figure 1.1: Outline of the methodology of the work in the thesis, from the identification of the key components to the results of the performed analysis.

2

Hood overslam

Closing a hood cautiously will not give any damages. However, when a hood is closed using a high force or velocity, which can be referred to as an overslam, it might be damaged. By simulating a hood overslam, displacements and contact forces at certain points of interest on the hood can be predicted. The results are used to analyze the influence of the impact on the parts neighboring the hood, such as the front lamps and the bumper. Capturing the dynamic behaviour of the event in the finite element model is critical for the final results to correlate well with reality.

2.1 Event and key component identification

The *hood seal* (blue in Figure 2.1) is the first component to come into contact with the hood during closing. The hood seal is made of relatively thin, low-stiffness rubber. In the XC90 model, the hood seal surrounds the engine bay with a constant, hollow cross section so that the inside forms a cavity. The hood seal is easily deformed. However, when the seal is compressed fast, the decreasing volume of the cavity causes the pressure to increase. This in turn results in a larger contact force between the seal and the hood. To keep the pressure in the hood seal at a moderate level, there are a number of vent holes enabling air venting in and out of the hood seal. Therefore the hood-to-seal contact force is relatively low for static cases, but is increased by dynamic effects.

The hood velocity during closing is further reduced by the *bump stops* (red in Figure 2.1). In the XC90 model, the bump stops are symmetrically mounted one on each side of the engine-bay, halfway between the windshield to the front bumper. The bump stops are solid components, consisting of rubber. This rubber is stiffer than the seal rubber, therefore it can withstand higher static loads without large deformations.

At the end of the downward motion of the hood it reaches the *latch* which is enclosed in the *locking house* (green in Figure 2.1). First, a rotational spring system connected to the latch starts damping the motion at initial latch contact. Depending on the velocity of the hood, it might get into contact with the bottom of the locking house. A locking mechanism, triggered by the rotation of the latch and induced after the hood hits the latch, locks the hood in closed position.

An accurate model for overslam analysis requires that these key components in the hood slam are studied deeper.

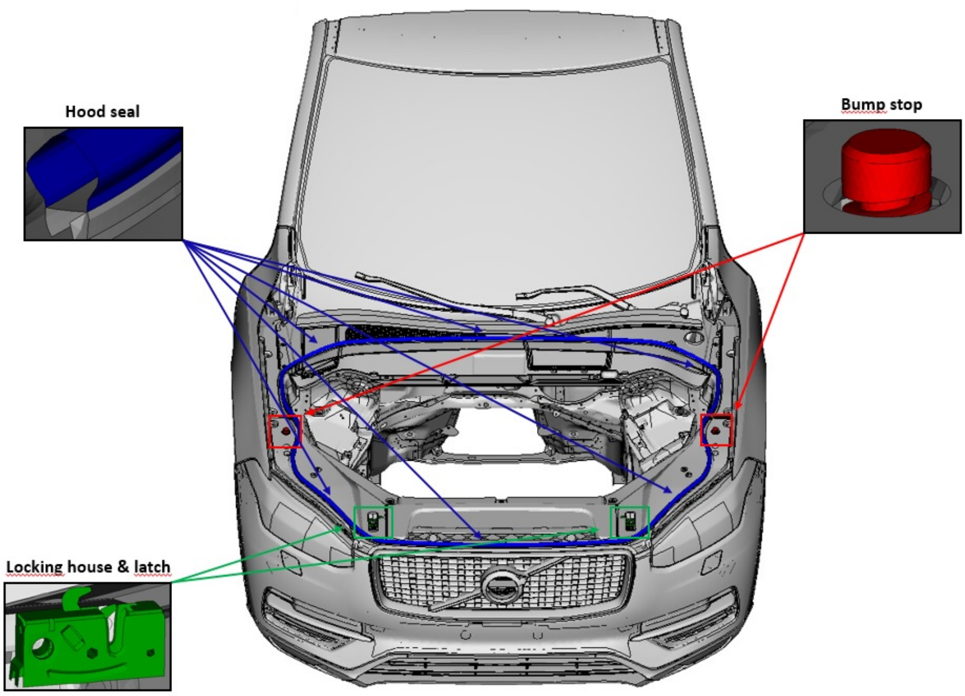

Figure 2.1: Volvo XC90 full front model with the hood removed and the key components highlighted.

2.2 XC90 model for hood overslam analysis

The finite element model used in the XC90 case study, displayed in Figure 2.1, includes the front car body, the hood, front bumper, lamps, bump stops and hood seal. The model is cut at the A-pillar. The front subframe and the engine are removed, leaving the engine bay empty.

2.3 Current hood overslam analysis method

In the current method for slam analysis at Volvo Cars, a Nastran model with a transient solution and an implicit integration scheme is used. The dynamic behaviour of the XC90 model for hood overslam analysis is considered reliable. However, contacts are in general not modeled, which means that the actual contact forces are disregarded. Further, bump stops and seals are modeled with nonlinear spring elements, making it hard to take changes in seal and bump stop geometry into account.

3

Bump stops

A bump stop of the XC90 is shown in Figure 3.1. It consists of a 72°IRH rubber. In use, the bump stop is driven into a mount on the fender carrier. The bump stops support a substantial part of the load of the hood in closed position and contribute to the damping of the hood in closing events.

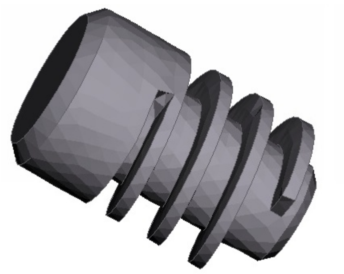

Figure 3.1: FE representation of an XC90 bump stop.

To avoid modeling of the bump stops as spring elements and meet the objective of keeping real component geometries, a material model that is able to capture the behavior of the rubber bump stops is needed.

3.1 Material model

There are numbers of models describing the deformation response of rubber materials. Some, like the Arruda-Boyce model, are based on statistical treatment of the macromolecular structure. In other models the stress-strain properties are derived from invariant-based continuum mechanics. The neo-Hookian, Mooney-Rivlin and Yeoh models are examples of the latter. These phenomenological models offer straightforward derivation of the material parameters through curve fitting and are valid for a wide range of strains, [3, 10].

The relatively simple three-parameter model for carbon black-filled rubber proposed by Yeoh [9] has been applied in applications similar to the subject for this thesis and its higher order terms allows for capturing the behavior of rubber at large strains, [4, 5].

The uniaxial stress-stretch relation in a compression or tension test, according to Yeoh, is given by:

$$\sigma = 2\left(C_{10} + 2C_{20}\Big(\frac{2}{\lambda} + \lambda^2 - 3\Big) + 3C_{30}\Big(\frac{2}{\lambda} + \lambda^2 - 3\Big)^2\right)\Big(\lambda - \frac{1}{\lambda^2}\Big) \tag{3.1}$$

where σ denotes the stress (force divided by initial area) and λ is the stretch ratio, defined as the deformed length divided by the initial length of the test specimen. The Yeoh parameters C_{10}, C_{20} and C_{30} are to be determined from material test data. A derivation of equation (3.1) can be found in appendix A.

3.1.1 Parameter identification from material test

Initial values of the Yeoh model parameters were derived from an ISO 7743 material compression test, performed by the rubber manufacturer Gislaved Gummi. Using the fitting procedure described in section A.4, the following numerical values of the Yeoh parameters were obtained:

$$C_{10} = 9.2 \cdot 10^{-4}\ GPa,\ C_{20} = -3.5 \cdot 10^{-4}\ GPa,\ C_{30} = 9.1 \cdot 10^{-5}\ GPa$$

To ensure the accuracy of the parameters at subsystem level, the force-displacement response of the bump stop and the supporting fender carrier was tested, see the following section.

3.1.2 Bump stop and fender carrier compression test

The bump stop and a cut-out part of the fender carrier were compressed between two parallel and flat steel plates as in Figure 3.2a. A load cell placed under the bottom plate measured the force. In the test, the specimens were loaded up to a load exceeding the expected maximum load of the hood overslam. The displacement was measured directly from the loading head displacement and applied with a rate corresponding to a strain rate of 1.5%/min, to minimize stresses due to viscous effects. Two different bump stop specimens were used, to account for variations, but no significant difference was observed between the two. Data were collected both with and without any mechanical conditioning of the bump stop. In the cases were mechanical conditioning was used, the bump stop was pre-loaded for three cycles of 10% of the maximum load during the test.

(a) Experimental setup for the compression test.

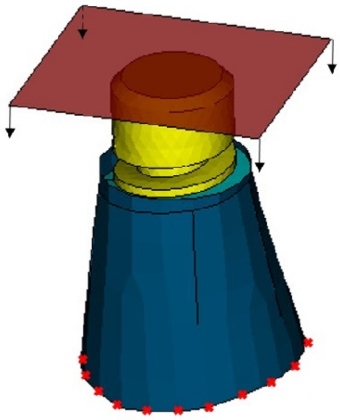

(b) FE model of the compression simulation with the prescribed displacement and the boundary conditions indicated.

Figure 3.2: Bump stop and fender carrier subsystem.

3.1.3 Correlation and parameter tuning

The bump stop-fender carrier structure was simulated in LS-Dyna, see Figure 3.2b, with the Yeoh parameters derived from the material test assigned to the bump stop. These simulations were delimited to the use of hyperelasticity and no viscous or inelastic effects following from mechanical conditioning of the material were implemented. Therefore the data for tests with no conditioning were used. In Figure 3.3, the resulting force-displacement curve is shown alongside the test result.

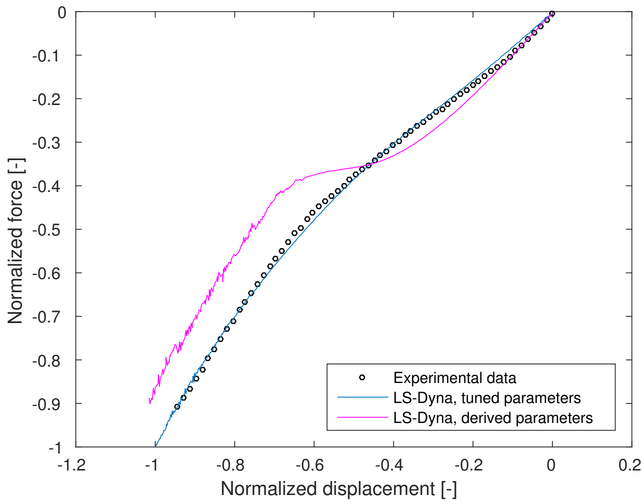

Figure 3.3: Experimental data and simulated force displacement curves for the compression.

As can be seen, there is a difference between the simulation with the derived parameters and the experimental data. To get a better fit, the parameters were varied in a scheme run in the software modeFRONTIER until a sufficiently accurate fit was obtained. The result from the simulation with the tuned parameters is also shown in Figure 3.3.

The Yeoh parameters were tuned to the following values:

$$C_{10} = 7.5 \cdot 10^{-4}\ GPa,\ C_{20} = -2.7 \cdot 10^{-4}\ GPa,\ C_{30} = 5.0 \cdot 10^{-4}\ GPa$$

3.2 Contact modeling in LS-Dyna

In reality, the bump stop rests upon the fender carrier. Use of standard contact formulations may result in a contact that instead makes the bump stop attached to the fender carrier from the bottom side, giving an unphysical bump stop behaviour. To ensure that the simulations operate correctly and the bump stop rests on the fender carrier, a tied contact for shell to solid elements was used. Also, initial penetration was allowed in the contact definition to prevent unphysical forces from arising. [7]

In computational applications, a large difference in stiffness between contact parts may result in stiffness losses. This is the case for the contact between the hood and the bump bump stops. The loss in stiffness can be compensated for by using of a soft contact formulation, which adds contact stiffness. Therefore a soft contact option was used in the bump-stop-to-hood contact. [8]

4

Hood sealing

A section of the hood seal can be seen in Figure 4.1. The seal acts as a damper during hood closings and may damp out sound and vibration. It also prevents dirt and dust from coming into the engine bay when the hood is in closed position. It consists of rubber that is softer and more foam-like than the bump stop rubber. The seal circumscribes the engine bay with a constant cross-section, forming a nearly closed cavity. However, there are vent holes evenly distributed along the seal circuit allowing for ventilation of air.

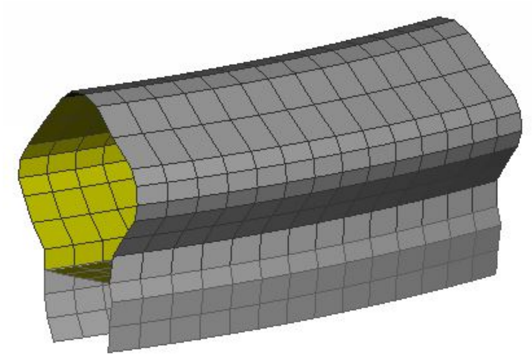

Figure 4.1: FE representation of an XC90 hood seal section.

4.1 Material model

The rubber of the hood seal was modeled with the Yeoh material model and the material parameters were obtained using the same procedure as for the bump stop in section 3.1.3. However, there were no material test data available for the seal rubber. Initial values of the Yeoh parameters were instead derived from a seal compression test performed at Volvo Cars. Similarly as for the bump stops, the parameters were tuned in a scheme run in modeFRONTIER until a good enough fit was obtained. The simulated force-displacement curve for the tuned parameters and the experimental data from the seal compression test are to be seen in Figure 4.2. A schematic of the simulation is shown as an inset in the figure.

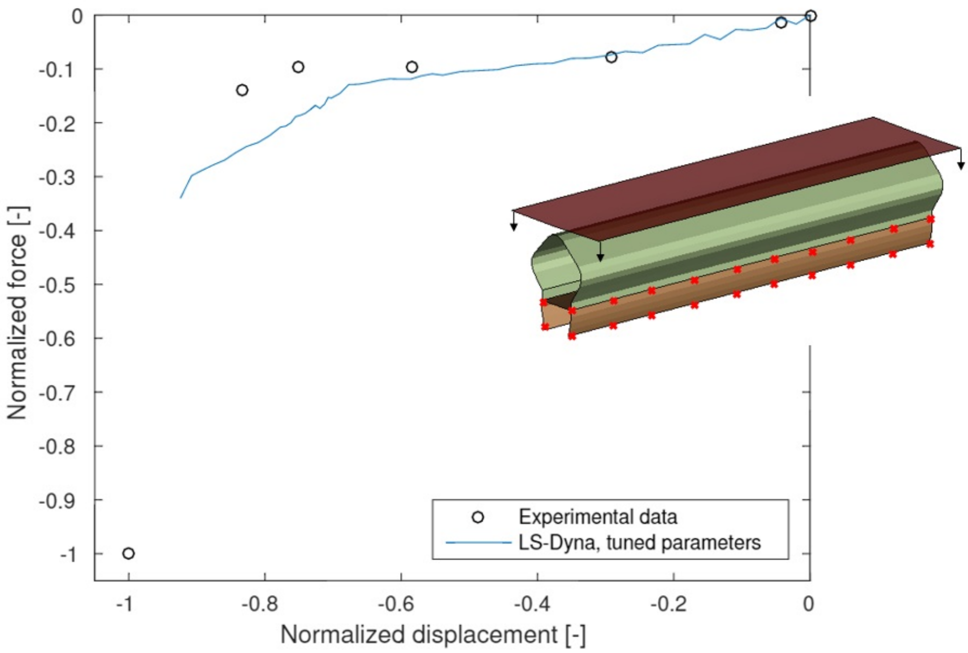

Figure 4.2: Experimental data and simulated curve.

The Yeoh parameters were tuned to the following values:

$$C_{10} = 4.4 \cdot 10^{-4}\ GPa,\ C_{20} = -1.2 \cdot 10^{-5}\ GPa,\ C_{30} = 2.7 \cdot 10^{-6}\ GPa$$

In the LS-Dyna simulations it was found that the hyperelastic material model caused the thin sheets of the seal geometry to swell, which is inconsistent with the assumption of incompressibility in the material model. This behavior was discovered when the cavity volume was observed to increase. Truncation errors of that sort occur when the solver cannot describe simulation inputs such as geometries or velocities accurately with finite-digit arithmetic. The truncation error is a function of the number of elements, or likewise the mesh size. For a large number of elements and a small mesh size, the last significant digit of so-called *single precision* simulations may be insufficient. The finite fixed number of digits used for single precision simulations in LS-Dyna is 7, whereas it is 16 digits for *double precision*. [6]

The problem occurred when single precision was being used and prevented by using double precision, but to the cost of an increased simulation time.

4.2 Seal cavity

The cavity of the hood seal was pressurized using an LS-Dyna airbag model. Airbag modeling in LS-Dyna originates from the gamma law gas equation of state (4.1) and the ideal gas law (4.2). [8]

$$p = (k - 1)\rho e \tag{4.1}$$

$$pV = nRT \tag{4.2}$$

Here p is the pressure, ρ is the fluid density, e is the specific internal energy of the gas and k is the ratio of specific heats $k = c_p/c_v$. V is the gas volume, n is the amount of substance, R is the relation $R = c_p - c_v$ and T the gas temperature.

A control volume was defined to occupy the same space as the seal cavity. Initially the pressure inside the cavity and the ambient pressure was set to 1 atm. Dry air of 20°C was assumed to obtain the necessary thermodynamic properties. The mass flow into the control volume was set to zero for the entire simulation. Overall the total vent hole area of the hood seal was estimated to 200 mm^2. The mass flow rate out of the control volume is calculated, according to [8], as:

$$\dot{m}_{out} = \mu_s \sqrt{2p_2\rho} \sqrt{\frac{k(Q^{\frac{2}{k}} - Q^{\frac{k+1}{k}})}{k-1}} \tag{4.3}$$

Here, Q is the relation between external pressure, p_e, and internal pressure, p_2, $Q = p_e/p_2$. The parameter μ_s is a shape factor that depends on the geometry of the vent holes, which can be varied in the interval $0 \leq \mu_s \leq 1$. A value of zero corresponds to an unvented sealing, whereas a value of one corresponds to perfect ventilation.

5

Locking mechanism

In the model of the lock, a rotational spring, describing the latch stiffness from physical testing, is activated at impact between the striker and latch. When the striker hits the bottom of the locking house and starts moving back up a sensor switch activates an additional rotational spring with a significantly greater stiffness, keeping the striker in locked position. The locking event in the model is briefly described in Figure 5.1, by three steps.

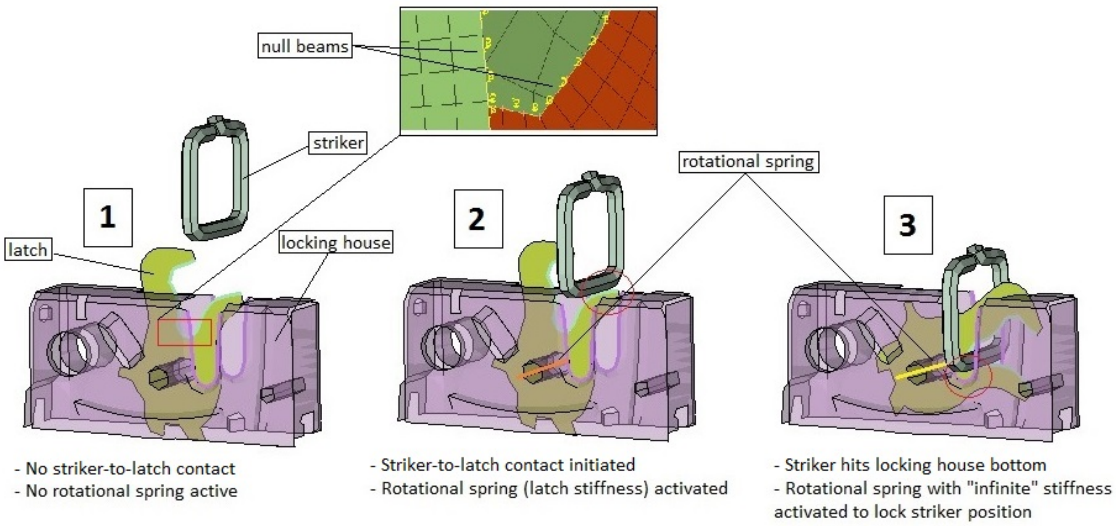

Figure 5.1: Three steps describing the function of the locking mechanism during closing in the LS-Dyna simulation.

Additional low-density null beams are attached at the edges of the latch and the locking house. These are used in the contact between the striker and the edge of the latch and locking house components. It creates an indirect contact to the latch and the locking house, see the magnified section in Figure 5.1. Also, the mesh is significantly refined at the contact regions of the locking components, to ensure the contact is handled properly.

Modeling the locking components in undeformable rigid materials simplifies the modeling of constraints related to the locking mechanism. To prevent oscillations due to numerical error from arising in the finite element model when the striker hits the latch, the rigid parts are modeled with a significantly lower density, $\rho = 10^{-10}\ kg/mm^3$. The modeling in undeformable bodies prevents the mesh refinement and the density decrease of the locking components from influencing the time step and no perceptable increase in computational time is expected.

6

Complete model

The modeling methods, material formulations and component structures described throughout chapters 3-5 were assembled and implemented in a full front finite element model consisting of the parts as described in section 2.2. The model, displayed in Figure 6.1 with defined coordinate system, was analyzed for overslam in LS-Dyna.

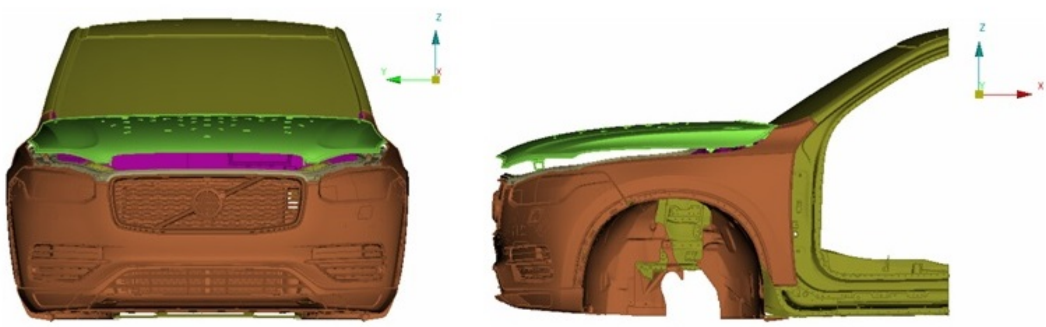

Figure 6.1: Complete model with defined coordinate system included.

6.1 Loads and boundary conditions

The model was fixed in all nodes at the cut just behind the A-pillar of the car and in the spring tower attachment position on both left and right hand side. An initial angular velocity, $\omega = {}^{v_{slam}}/_{r}$, around the hinge line of the hood, was applied onto all nodes of the hood. Here, v_{slam} is the slam velocity in negative z-direction at the front edge of the hood and r is the distance in x-direction from the hinge line to the front edge of the hood. Initial displacements, corresponding to a small hood opening angle, were applied to the hood nodes. Gravity effects were judged small enough to be neglected in the simulations.

6.2 Unknown parameters

The influence of the parameters with the greatest uncertainty and somewhat significant effect on the result has been investigated. These were the vent hole *shape factor* of the airbag used in the sealing and the *static friction coefficient* of the seal-to-hood contact.

The maximum *overtravel* at the four points defined in Figure 6.2, was evaluated at a velocity low enough not to allow for any contact between the hood and the lamps but still high enough to be considered an overslam. Here, the overtravel is defined as the portion of the displacement in negative z-direction that exceeds the nominal closed hood position. In Tables 6.1-6.2, the maximum overtravel, normalized to the test data, is presented.

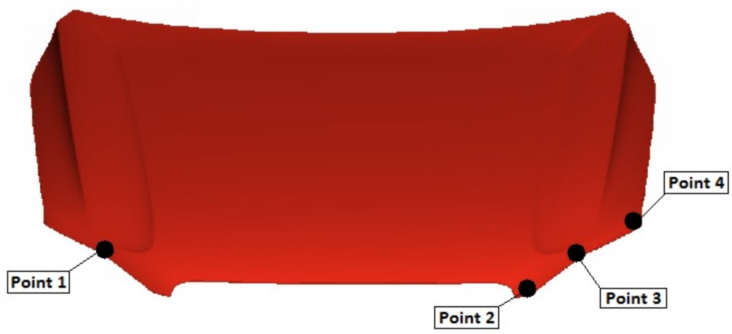

Figure 6.2: Hood points at which the displacements are measured.

The shape factor of the airbag vent holes used in the sealing, which controls the mass flow out of the control volume, as described in chapter 4.2 was varied in the interval $0.3 \leq \mu_s \leq 0.7$. The results for overtravel of the test points on the hood for the different parameter values are displayed in Table 6.1 along with results from test and from the current Volvo model (Nastran).

Shape factor, μ_s [-]	Source	Max hood overtravel [-]			
		P1	P2	P3	P4
-	Test	1.00	1.00	1.00	1.00
-	Nastran	1.15	1.06	1.07	1.02
0.3	LS-Dyna	1.12	0.976	1.05	1.21
0.4	"	1.14	0.985	1.05	1.22
0.5	"	1.15	0.994	1.07	1.23
0.6	"	1.16	1.00	1.07	1.23
0.7	"	1.16	1.01	1.07	1.23

Table 6.1: Varied shape factor, μ_s and fixed static friction coefficient, $\mu_f = 0.1$. The maximum hood overtravel is normalized to the test data.

The static friction coefficient in the seal to hood contact is investigated within the interval $0.1 \leq \mu_f \leq 0.9$, based on recommendations from Volvo Cars. The overtravel results for the different parameter values are displayed in Table 6.2 and compared with results from test and from the current Volvo model (Nastran).

Static friction coefficient, μ_f [-]	Source	Max hood overtravel [-]			
		P1	P2	P3	P4
-	Test	1.00	1.00	1.00	1.00
-	Nastran	1.15	1.06	1.07	1.02
0.1	LS-Dyna	1.13	0.986	1.05	1.21
0.5	"	1.10	0.980	1.03	1.19
0.9	"	1.09	0.975	1.03	1.19

Table 6.2: Varied static friction coefficient, μ_f and fixed shape factor, $\mu_s = 0.4$. The maximum hood overtravel is normalized to the test data.

Overtravel results from three out of four observed points indicate that low values of the vent hole shape factor and high values of the static friction coefficient give better correlation to test data. However, a shape factor value of zero would implicate a completely unvented sealing, which is not the case in this scenario. Moreover, the overall behavior of the force in the seal during the simulation, as in Figure 6.3, does not correspond to the current Volvo model behavior for too low shape factors. A shape factor of 0.4 results in a somewhat uniform offset to the current Volvo model seal force for the entire time interval, still correlating well with overtravel test data. Therefore it was chosen to be used in the model.

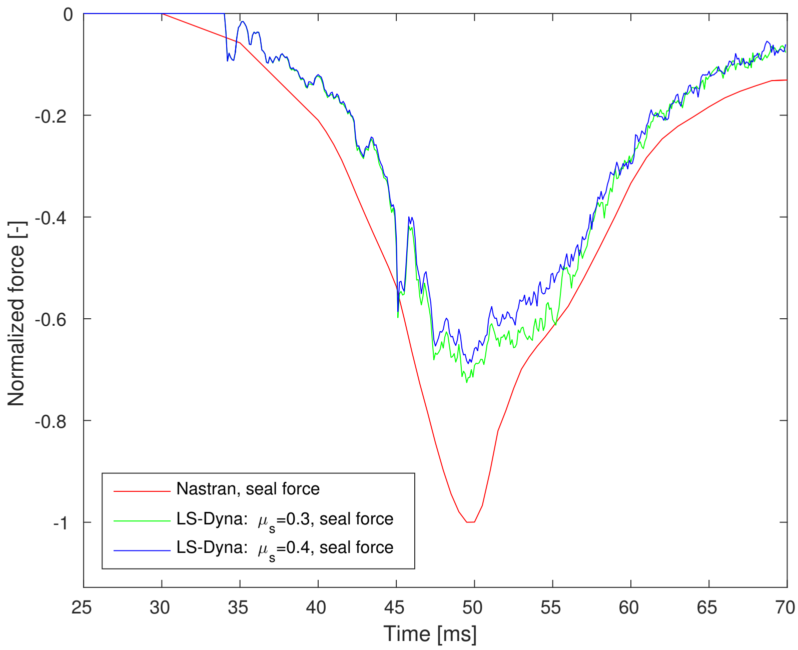

Figure 6.3: Z-component of the force on the seal.

The static friction coefficient was found to be less influential on the results. However, slightly better correlation to test data was obtained for higher static friction values. Therefore a static friction coefficient of 0.9 was chosen for the model.

7

Output from complete model

The airbag shape factor, $\mu_s = 0.4$ and seal static friction coefficient, $\mu_f = 0.9$, were obtained in chapter 6. This set of parameters is implemented in the developed LS-Dyna model.

Here two different velocities are used to obtain the results. One velocity low enough to ensure no contact between the lamp and hood and one high velocity at which there is contact between these two parts. The low velocity is used in all cases but the hood-to-lamp contact force of section 7.2, where the high velocity is used.

7.1 Hood overtravel

In Table 7.1 the maximum hood overtravel obtained from physical testing, the current Volvo model (Nastran) and the developed LS-Dyna model are tabulated. The results are normalized to the test results. Figure 7.1 shows the displacement in the z-direction of hood point 3, with the time interval in which the maximum displacement is reached magnified.

Source	Max hood overtravel [-]			
	P1	P2	P3	P4
Test	1.00	1.00	1.00	1.00
Nastran	1.15	1.06	1.07	1.02
LS-Dyna	1.09	0.975	1.03	1.19

Table 7.1: Maximum hood overtravel for test, Nastran and LS-Dyna.

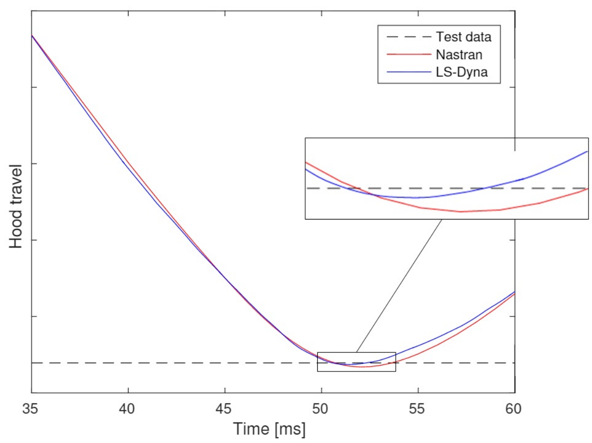

Figure 7.1: Hood travel of point 3.

The maximum overtravel of the LS-Dyna model were 9.0 %, 2.5 %, 3 % and 19 % from the test data at point 1 to 4, respectively. In all cases but point 2, the LS-Dyna model was conservative compared to test. The LS-Dyna model was closer to the test data than the current Volvo model at point 1, 2 and 3, whereas the deviation at point 4 exceeded the current Volvo model.

At point 1, 2 and 3, the hood z-travel plots look relatively similar, with a smooth appearance as in Figure 7.1 above. The plot of point 4 presented below in Figure 7.2, on the other hand, is less smooth. It is likely that this behavior originates from the fact that the locking house is modeled with a rigid material.

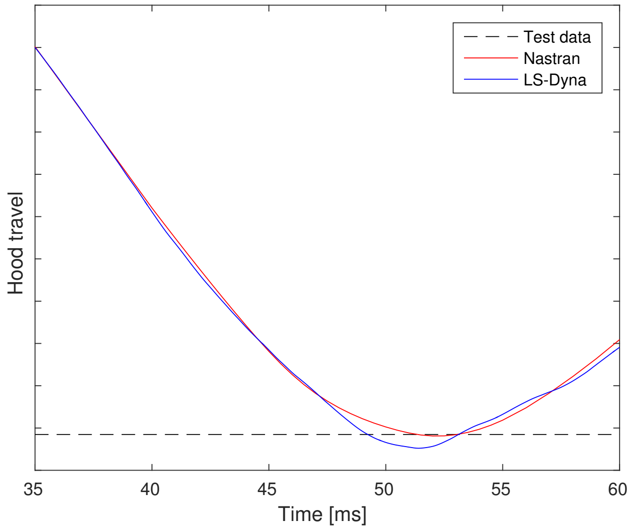

Figure 7.2: Hood travel of point 4.

When the striker hits the bottom of the locking house, as in Figure 7.3a, point 2-4 starts to rotate around the contact point. Since the locking house is modeled with a rigid material this rotation cannot initiate as smoothly as if the locking house would be modeled with a deformable material. Point 4 is the most distant from the contact point of the striker and the locking house, consequently the unsmooth behavior is more pronounced in point 4 than in point 2 and 3. The rotation at point 4 may be further enhanced by the fact that a greater portion of the total weight of the hood is acting in that point.

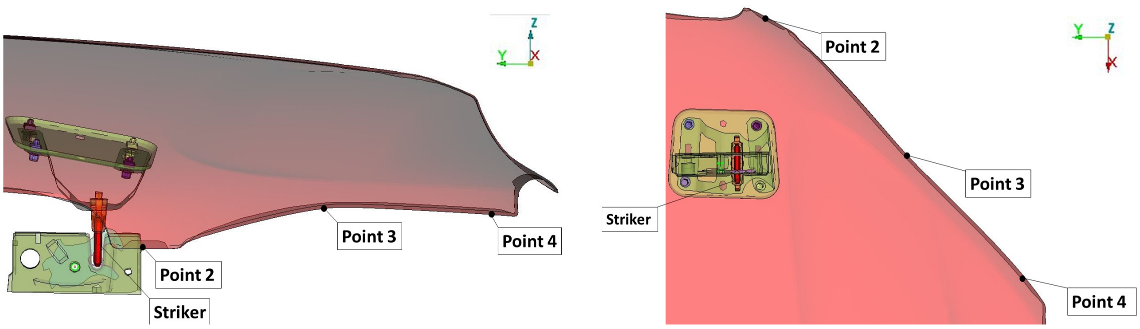

(a) Front view. **(b)** Bottom view.

Figure 7.3: Hood point and striker positions.

What is more, due to the shape of the striker the rotational stiffness of the hood around the y-axis exceeds the rotational stiffness around the x-axis. This is also likely to be the reason why the LS-Dyna underpredicts the overtravel at point 2.

7.2 Hood-to-lamp contact force

Two different slave contact forces are evaluated. One between the hood and the entire lamp and the second one between the hood and the lamp lens only, as in Figure 7.4.

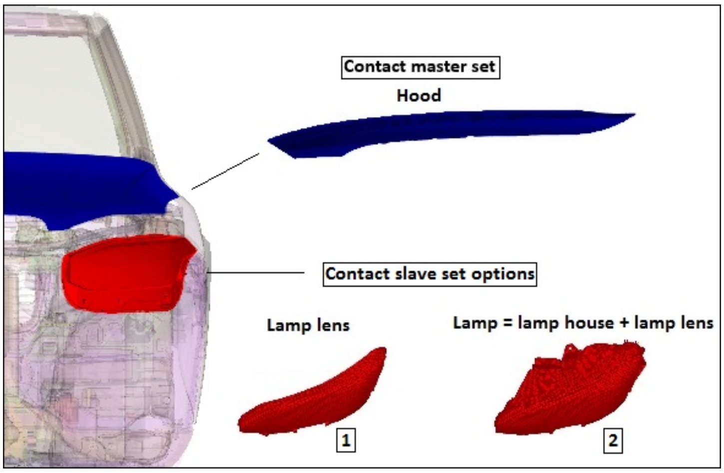

Figure 7.4: Slave sets of the hood-to-lamp contact forces.

In Table 7.2 both forces are shown for the LS-Dyna simulation.

Source	Maximum contact force, hood to lamp [N]	Maximum contact force, hood to lamp lens [N]
LS-Dyna	42.8	$3.95 \cdot 10^{-3}$

Table 7.2: Hood-to-lamp contact forces.

The force between the hood and the lamps during the overslam cannot be compared to any test data or alternative model. However, it illustrates the possibility of quantifying the forces acting on different parts. Clearly, most of the contact force is absorbed by the lamp housing in this case, whilst a very small fraction of the total force is found in the actual lamp lens. Naturally this behavior depends on the geometry of the lamps and the hood. The contact formulation in LS-Dyna allows for defining even smaller slave sets and potential to determine precisely where the contact is initiated.

7.3 Bump stop and hood seal forces

The forces in the bump stops and in the seal are extracted as the contact forces in the contact to the hood. The models are nearly symmetric about the mid-axis and the difference between the force acting on the left and right hand side bump stop is insignificant. Therefore the results are presented for the left hand side only. The contact force between the hood and the left bump stop appears to the right in Figure 7.5. The hood-to-seal force is shown to the left. In both cases the developed LS-Dyna model, with and without airbag modeling of the seal cavity, is plotted alongside the current Volvo model (Nastran).

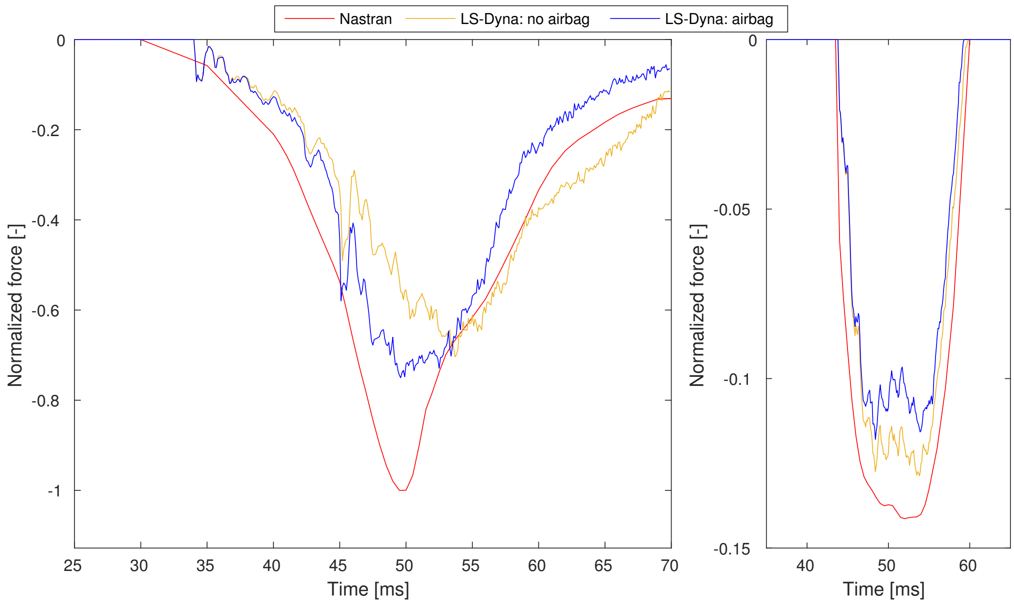

Figure 7.5: Force in z-direction on the seal (left) and one bump stop (right). N.B., the seal and bump stop curves are normalized to the same value, and the axis scaling differs.

It is evident that the sealing and bump stops are interacting. A higher force in the seal implies a decreased force in the bump stops. Conversely, a decreased seal force means an increased bump stop force. The improved behavior of the airbag usage in the seal cavity modeling is apparent with a time dependence more similar to the current Nastran model. A difference between the LS-Dyna models and the Nastran model can be observed. The force magnitude of the Nastran model is exceeding the force magnitude of the LS-Dyna model in both the seal and the bump stop. That is likely due to the idealized modeling of these components with discrete spring elements in the Nastran model. Whereas the seal of the LS-Dyna model, with the actual geometry kept, cannot absorb as much force since it is bending and twisting.

7.4 Hood velocity components

The velocity components in the x- and z-direction at the midpoint of the front edge of the hood (y=0 position) are plotted for the developed LS-Dyna model in Figure 7.6. In the plot the velocity components in the x- and z-direction of the current Volvo model (Nastran) are also shown. Further, the x- and z-velocity components of a version of the developed LS-Dyna model with the actual density of the rigid lock parts kept, are shown.

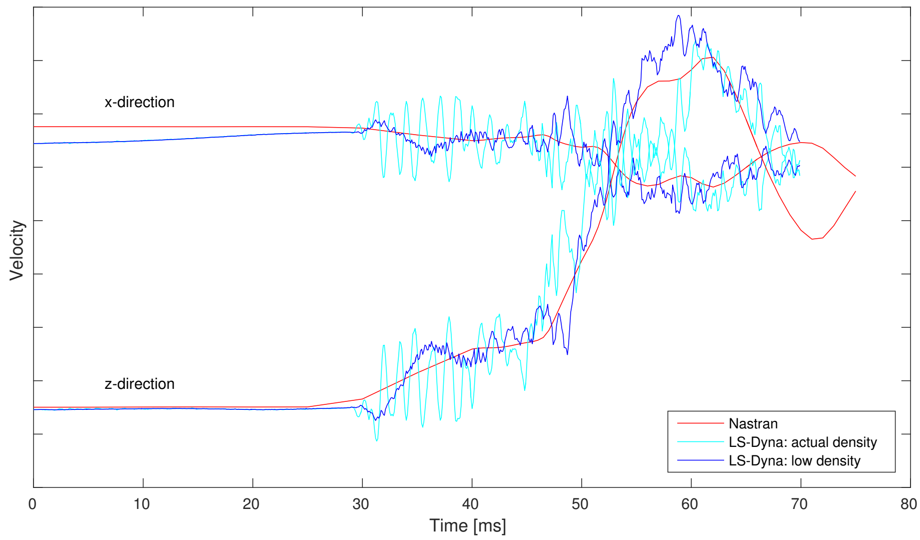

Figure 7.6: Velocity of the mid-front hood point.

Comparing the velocity components of LS-Dyna model with the current Volvo model, the overall behavior is the same. However, oscillations can be observed in the LS-Dyna model results. The smoother appearance of the Nastran curves is not surprising, since an implicit integration scheme is used as opposed to the explicit scheme used in LS-Dyna. Implicit time integration is numerical stable whereas explicit time integration is only stable if sufficiently small timesteps are taken. This reasoning also applies to the the force plots of Figure 6.3 and 7.5. The oscillations observed in the LS-Dyna simulations may be eliminated by using smaller time steps or appropriate damping in the model.

The difference of the LS-Dyna model run with the actual density and the low density of the rigid lock parts, as described in chapter 5 is also demonstrated in the plot. Clearly, the oscillations is diminished by lowering the density.

7.5 Computing power performance

The LS-Dyna model was tested using single precision (SP) and double precision (DP) computation. In Table 7.3 the simulation times are presented for a single precision LS-Dyna run, a double precision LS-Dyna run and a standard Nastran run, respectively. The number of CPUs used in each simulation follows the Volvo Cars standard guidelines. The current Volvo model (Nastran) is used as the reference.

Source	Simulation time [h, min]	Simulation time [% of Nastran]
Nastran	6 h, 25 min	100 %
LS-Dyna (SP)	3 h, 5 min	48 %
LS-Dyna (DP)	3 h, 55 min	61 %

Table 7.3: Simulation times for the overslam analysis with single precision LS-Dyna, double precision LS-Dyna and the current Volvo model (Nastran).

As can be seen in Table 7.3, the use of double precision adds on 27 % in simulation time to the single precision simulation. Still it is far less computationally intensive than the current Volvo model (Nastran). Using LS-Dyna for overslam analysis reduces the computational time by 52 % and 39 % for single precision and double precision simulations respectively, compared to the current Volvo model. Single precision runs are preferable regarding computational time. However, single precision has been proven insufficient in terms of numerical stability in simulations that includes rubber models. Therefore double precision has been used in the thesis.

To get a picture of the impact of the truncation error in the single precision LS-Dyna simulations, the hood overtravel results have been compared to the double precision LS-Dyna simulation results and test data in Table 7.4.

Source	Max hood overtravel [-]			
	P1	P2	P3	P4
Test	1.00	1.00	1.00	1.00
LS-Dyna (SP)	0.988	0.916	0.966	1.10
LS-Dyna (DP)	1.09	0.975	1.03	1.19

Table 7.4: Maximum hood overtravel for test, single precision LS-Dyna and double precision LS-Dyna.

At three out of four observed points, the overtravel is underpredicted in the single precision simulations. That is likely due to the increased volume of the seal cavity that has been observed in the single precision simulations. In the single precision simulation the hood gets into contact with the seal precedent to what is the case in the double precision simulation. Therefore the hood velocity reaches zero at an earlier point. The non-conservative results of the single precision simulation motivates the use of double precision.

8

S90 model

The method developed in the case study of the Volvo XC90 is implemented in a finite element model of the Volvo S90 to investigate the robustness of the modeling approach. There are a few differences between the XC90 and the S90 that have to be considered. The seal has open ends and does not form a closed cavity so no airbag modeling is needed. The S90 has three bump stops of the same kind as the two bump stops in the XC90. Two which are mounted similarly as in the XC90, at right and left hand side of the engine-bay respectively and the third one mounted in the middle front.

Moreover, the S90 has multi-link hinges, which means that the axis of rotation for the hood closing motion has to be calculated. A minor error in the calculation of the momentary rotation axis has been observed in the initial opening rotation of the LS-Dyna model. In Figure 8.1, the misaligned rotation axes of the links are highlighted.

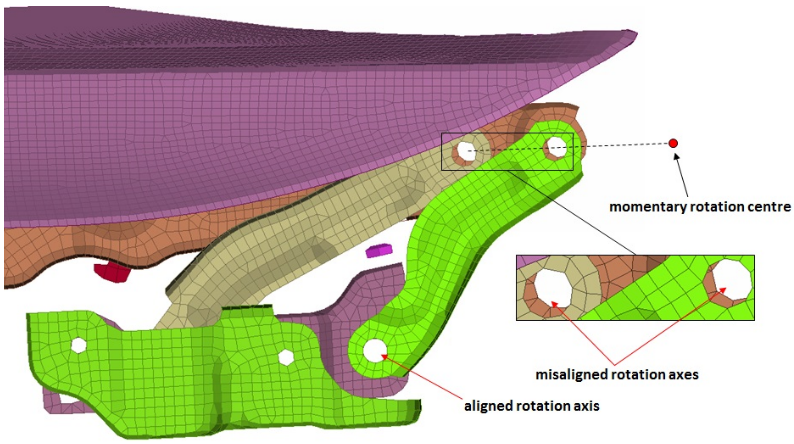

Figure 8.1: Multi-link hinge in S90 with the misaligned link rotation axes enlarged.

However, the rotating motion of the hood around the calculated rotation axis is not notably affected by the misalignment. The impact of the misalignment on the hood overtravel has not been studied deeper.

Physical test data of hood displacement in one hood point is available for the S90, hence it is used in the comparison. The test was performed at a velocity enough to obtain contact between the hood and lamps. There are uncertainties of the exact hood point position used in the test and the test data are somewhat inconsistent, consequently the results tabulated in Table 8.1 are not as uniform as in the XC90 case study. The displacement in the z-direction of the observed hood point is shown in Figure 8.2 for the time interval where the overtravel reaches its maximum value.

Source	Max hood overtravel [-]
Test	1.00
Nastran	2.44
LS-Dyna	1.43

Table 8.1: Maximum hood overtravel.

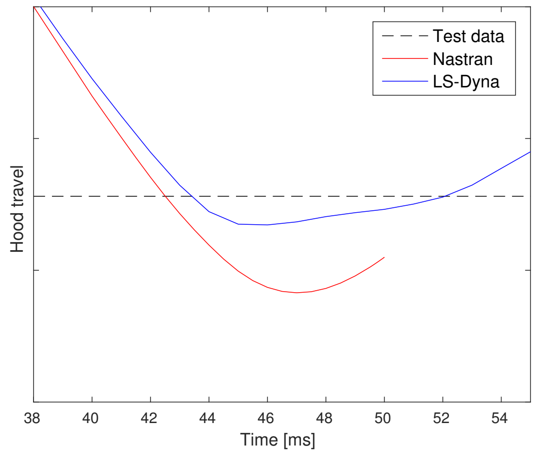

Figure 8.2: Hood travel for the time interval where the overtravel reaches its maximum value.

From Figure 8.2, the main advantage with the developed method in LS-Dyna can be observed. The LS-Dyna model clearly captures the contact that was present in the physical test and the motion is slowed down faster. As in the XC90 case, the LS-Dyna S90 model overpredicts the overtravel results, compared to test data. The results obtained from simulations of the LS-Dyna S90 model deviates by 43 % from test results. The deviation from test data is significantly larger for the current Volvo model (Nastran). However, the only possible observation with the current Volvo model is whether there will be a contact or not.

9
Discussion

9.1 Model and results

Even though damping may seem like an obvious topic to consider during a hood closing event, it has not been investigated further. For the modeling to be general, artificial quantities such as damping have been avoided to as great extent as possible. Using damping may have a false positive effect on the results and therefore it may not be applicable in other models. Nevertheless, the results could probably be improved by the use of damping.

In the XC90 model, the initial opening of the hood can easily be performed by manually rotating it around the hinge line. However, more complex hood hinges such as the S90 multi-link hinge, require the momentary rotation center to be determined. In the thesis, this momentary rotation center was determined with a small error. The error had no major effect on the results.

The simulation time is reduced by up to 52 % compared to the current Volvo method. Even though it is hard to quantify, the modeling time is also believed to be reduced by use of the developed LS-Dyna modeling method. That is mainly due to the fact that more or less compatible models from CAE safety departments can be used but also because less additional files need to be imported into the model.

9.2 Material model

The hyperelastic rubber material model is computationally intensive and needs to be evaluated with more significant figures to get good results. Using the Yeoh model and single precision settings in LS-Dyna causes the thin sheets of the hood seal to swell. Therefore double precision is used for all results except one of the simulations in the comparison of single and double precision. Simpler material models with no need of double precision, such as a bilinear elastic material model, could possibly be used without having too significant effect on the results.

The Yeoh model is used for both rubber components, i.e. bump stop and seal. The material model is developed for carbon black-filled rubber, thus it is well suited for the bump stop rubber but less suitable for the softer seal rubber. The deformation behavior of the seal may be better captured by a material model for softer rubber or a foam model. However, comparing the influence on the results by the airbag model and the hood seal material formulation, respectively, the seal cavity seems to have greater impact on the overall sealing behaviour during the closing event.

There are some uncertainties regarding the test data of the seal compression test. Since the test was performed prior to the start of the thesis it could not be controlled properly. Consequently there is a risk that the finite element submodel that was used to correlate the hood seal material model differs from the test setup.

The viscoelastic properties of the rubber have not been investigated deeply and are not included in the developed LS-Dyna model. A further investigation of the viscoelastic behavior of the seal and bump stop rubber may result in a model that better captures the dynamics of these components.

Even though finite element modeling is well developed, the results of the bump stop compression test highlights the difficulties in applying complex material models into a CAE environment. The parameters of the Yeoh model derived from the standardized material test are to be considered accurate for the rubber material solely. However, implementing the Yeoh model into a CAE substructure, as in the compression test performed in the thesis, these parameters must be somewhat tweaked to capture the correct behaviour.

9.3 Seal cavity and airbag modeling

The fundamental underlying mechanics of a vented seal and an airbag is similar. For the XC90 seal cavity, the ratio of the total volume and the vent hole area is of the same magnitude as for a typical airbag. Therefore the use of the LS-Dyna airbag model is well motivated. In the simulation, the mass flow rate into the cavity of the hood seal is set to zero. It means that after the cavity volume has been compressed to its minimum and it starts to increase, the pressure in the seal will be erroneous. However, in the overslam load case it is assumed that the maximum overtravel and the minimum cavity volume occur simultaneously. Errors appearing after this point of time are thus of less importance.

When a hood is closed, a pressure is built up in the engine bay. It could probably have been modeled in a way similar to the seal cavity but, since it is deemed to have a negligible effect on the overall motion of the hood, it has been neglected in the analysis.

10 Future work

The hyperelastic rubber model used to describe the rubber material properties in the thesis is not fully compatible with the hood seal. A material model developed for foam-like soft rubbers should therefore be further investigated to improve the modeling of the hood seal. Moreover, accounting for viscous and inelastic effects in the material modeling of the bump stop rubber would make the complete model more realistic.

Testing the modeling method developed for hood closing on doors and trunklids is suggested to further facilitate the handling of similar load cases. A case study on another model with a closed seal cavity would also give useful information about the accuracy of the seal airbag modeling approach.

To improve the efficiency and create faster models for explicit simulations, selective mass scaling and other alternative ways to decrease the simulation times should be further investigated. A script to automate the initial opening motion of the hood using a kinematic simulation tool would also help to streamline the work with closing analyses.

There are more sophisticated airbag models in LS-Dyna than the one used in this project. Other control volume-based models or corpuscular formulations may improve the seal cavity modeling and provide an improved description of the seal dynamics. Physical test data on the venting characteristics of the seal would facilitate such attempts.

The outlying value of the hood overtravel at point 4 suggests that a modal analysis of the hood could contribute to the understanding of the hood deformation behavior.

It should be considered to investigate possibilities of finding a workaround for the use of double precision calculations, without acquiring numerical errors due to the rubber sheets in the hood seal.

11

Concluding remarks

A modeling method for performing hood slam analysis in LS-Dyna has been developed.

The method developed allows for evaluation of the contact force between the hood and the lamp lens directly, which is not possible in the current Volvo method. Also the contact force between neighboring components, which may have an indirect effect on the load level of the lamp lens itself, may be evaluated. Modifications to the analysis can be done with ease. The model is well adapted to account for future changes of the components, hence no new component tests are needed. Instead the same material model may be implemented, independent on component geometry.

The visual comprehensibility is improved using the developed LS-Dyna modeling method compared to the current Volvo model. First of all, fewer nonlinear spring elements are used which means less visual disturbance when animating the simulation results. Also, mechanisms in the model are modeled in a more realistic way, which makes it easier to comprehend the results for someone who has less experience with finite element modeling.

Results of hood displacements show that the developed LS-Dyna model is better correlated to test data at three out of four hood points, compared to the current Volvo model for slam analysis. The model is conservative at three out of four observed points.

Compared to the current Volvo method, the simulation time is reduced by 39 % using double precision settings and by 52 % using single precision. The LS-Dyna simulations take three to four hours, which makes it possible to run the simulation and analyze it during the same work day. It is an important aspect to consider to enable an effective CAE process.

Judging by the results in the verification study of the S90 model, the methodology is also general enough to be applicable on different models. Though, depending on the model, more or less extensive modifications is needed.

References

[1] P.E. Austrell. “Modeling of Elasticity and Damping for Filled Elastomers”. PhD thesis. Lund University, 1997, p. 222. ISBN: 0281-6679.

[2] S.E. Bechtel and R.L. Lowe. *Fundamentals of Continuum Mechanics*. Boston, MA: Academic Press, 2015.

[3] M.C. Boyce and E.M. Arruda. “Constitutive Models of Rubber Elasticity: A Review”. In: *Rubber Chemistry and Technology* 73.3 (2000), pp. 504–523. DOI: 10.5254/1.3547602.

[4] O.J. Centeno Gil. “Finite Element Modeling of Rubber Bushing for Crash Simulation - Experimental Tests and Validation”. Master’s thesis. Lund University, 2009.

[5] P. Håkansson. “Finite Element Modeling of a Rubber Block Exposed to Shock Loading”. Master’s thesis. Lund University, 2000.

[6] Yih-Yih Lin. “Performance of LS-DYNA with Double Precision on Linux and Windows CCS”. In: *6th European LS-DYNA Users’ Conference* (2007), pp. 3.107–3.111.

[7] *LS-Dyna Keyword User’s Manual*. Livermore Software Technology Corporation. 2016.

[8] *LS-Dyna Theory Manual*. Livermore Software Technology Corporation. 2016.

[9] O.H. Yeoh. “Characterization of Elastic Properties of Carbon-Black-Filled Rubber Vulcanizates”. In: *Rubber Chemistry and Technology* 63.5 (1990), pp. 792–805. DOI: 10.5254/1.3538289.

[10] O.H. Yeoh and P.D. Fleming. “A new attempt to reconcile the statistical and phenomenological theories of rubber elasticity”. In: *Journal of Polymer Science Part B: Polymer Physics* 35.12 (1997), pp. 1919–1931. DOI: 10.1002/(SICI)1099-0488(19970915)35:12<1919::AID-POLB7>3.0.CO;2-K.

A

Rubber elasticity

A derivation of the Yeoh model [9] and the procedure used to obtain the parameters follow in this appendix.

A.1 Kinematics: Deformation tensors

First, the deformation tensors are defined. [2]

Bodies can be seen as sets of particles. Each particle P of a body $\mathcal{B}$ is assumed to have a one-to-one correspondence with the real numbers X, Y, Z in a region of the Euclidean 3-space $\mathcal{R}^3$, given that the one-to-one mapping from the body onto the domain of $\mathcal{R}^3$ is invertible and differentiable as many times as needed. A body is seen in the region of $\mathcal{R}^3$ that it occupies at an instant of time t, the configuration. Let the capital letters X, Y, Z and $\mathbf{r}_0$ denote the reference configuration, the lower-case letters x, y, z and $\mathbf{r}$ the deformed configuration respectively. The vectors $\mathbf{r}_0$ and $\mathbf{r}$ refer to the position of the place occupied by a particle P at time $t = 0$ and time t, respectively see Figure A.1.

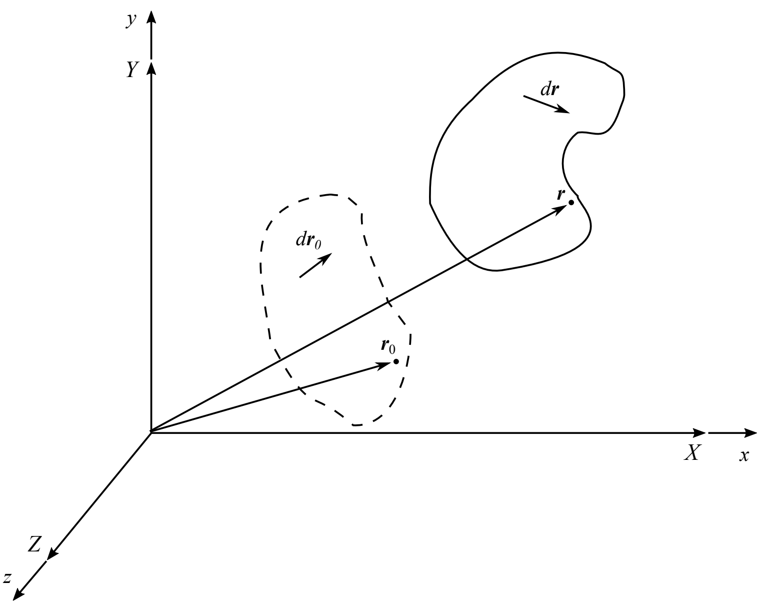

Figure A.1: Deformable body in reference and deformed configuration with material line elements, $d\mathbf{r}_0$ and $d\mathbf{r}$, defined.

The deformation of a body may be described by a mapping of each particle in the body from the reference configuration to the deformed configuration. On matrix form:

$$\begin{bmatrix} x \\ y \\ z \end{bmatrix} = \begin{bmatrix} x(X,Y,Z,t) \\ y(X,Y,Z,t) \\ z(X,Y,Z,t) \end{bmatrix} \iff \mathbf{r} = \mathbf{r}(\mathbf{r}_0, t) \tag{A.1}$$

By differentiating equation (A.1), a relation that describes how the length and direction of a material line element, as in Figure A.1, changes under deformation can be obtained:

$$\begin{bmatrix} dx \\ dy \\ dz \end{bmatrix} = \begin{bmatrix} \frac{\partial x}{\partial X} & \frac{\partial x}{\partial Y} & \frac{\partial x}{\partial Z} \\ \frac{\partial y}{\partial X} & \frac{\partial y}{\partial Y} & \frac{\partial y}{\partial Z} \\ \frac{\partial z}{\partial X} & \frac{\partial z}{\partial Y} & \frac{\partial z}{\partial Z} \end{bmatrix} \begin{bmatrix} dX \\ dY \\ dZ \end{bmatrix} \iff d\mathbf{r} = \mathbf{F} d\mathbf{r}_0 \tag{A.2}$$

where the second order tensor (matrix) $\mathbf{F}$ is known as the deformation gradient.

Introducing the following definitions of the right and left Cauchy-Green deformation tensors respectively:

$$\mathbf{C} = \mathbf{F}^T\mathbf{F}, \;\; \mathbf{B} = \mathbf{F}\mathbf{F}^T \tag{A.3}$$

The right and left Cauchy-Green deformation tensors have the following invariants:

$$\begin{cases} I_1 = tr(\mathbf{C}) = tr(\mathbf{B}) = \lambda_1^2 + \lambda_2^2 + \lambda_3^2 \\ I_2 = \frac{1}{2}(tr(\mathbf{C})^2 - tr(\mathbf{C}^2)) = \frac{1}{2}(tr(\mathbf{B})^2 - tr(\mathbf{B}^2)) = \lambda_1^2\lambda_2^2 + \lambda_1^2\lambda_3^2 + \lambda_2^2\lambda_3^2 \\ I_3 = det(\mathbf{C}) = det(\mathbf{B}) = \lambda_1^2\lambda_2^2\lambda_3^2 \end{cases} \tag{A.4}$$

where the square root of the principal values of the right and the left Cauchy-Green deformation tensors, $\mathbf{B}$, are equal to the principal stretches, λ_i [1].

A.2 The Yeoh model

In the following the Yeoh model is derived and fitted to the experimental data using the procedure outlined by Austrell [1].

The Yeoh material model is hyperelastic, and therefore based on the idea that the stresses can be derived from a strain energy function. It is convenient to express the strain energy function, W, as dependent on the left Cauchy-Green deformation tensor $\mathbf{B}$. For an isotropic material however, the state of deformation is fully determined by the principal stretches:

$$W = W(\mathbf{B}) \Rightarrow W = W(\lambda_1, \lambda_2, \lambda_3) \tag{A.5}$$

Instead of solving the eigenvalue problem to obtain the principal stretches the strain energy function can, more conveniently, be expressed in terms of the invariants in equation (A.4). A common formulation of the strain energy function is the polynomial form:

$$W = W(I_1, I_2, I_3) = \sum_{i,j,k=0}^{\infty} C_{ijk} = (I_1 - 3)^i (I_2 - 3)^j (I_3 - 1)^k \tag{A.6}$$

The third invariant governs the volume change, so if incompressibility is assumed the strain energy function reduces to:

$$W = W(I_1, I_2) = \sum_{i,j=0}^{\infty} C_{ij} = (I_1 - 3)^i (I_2 - 3)^j \tag{A.7}$$

Yeoh concluded that for carbon black-filled rubbers the dependence on the first invariant, I_1, is far stronger than on the second, I_2. Truncating the series after three terms yields:

$$W = W(I_1) = C_{10}(I_1 - 3) + C_{20}(I_1 - 3)^2 + C_{30}(I_1 - 3)^3 \tag{A.8}$$

A.3 Tension and compression tests

The stretch in a tension or compression test is defined:

$$\lambda = \frac{L + \delta}{L} \tag{A.9}$$

where L denotes the undeformed length and δ the prescribed displacement. With the principal axes defined according to Figure A.2.

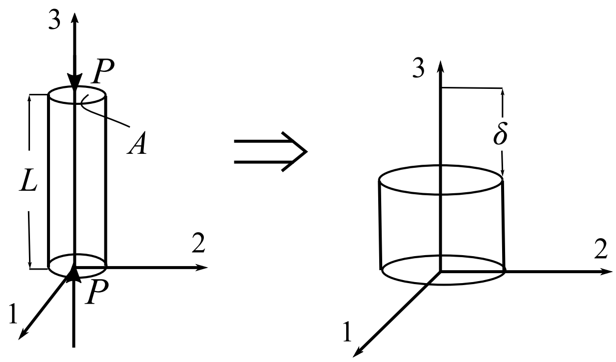

Figure A.2: Principal axes in a compression test.

In order to satisfy incompressibility ($det(\mathbf{F}) = 1$) the product of the principal stretches must equal one, so that:

$$\begin{cases} \lambda_1 = \lambda_2 = \frac{1}{\sqrt{\lambda}} \\ \lambda_3 = \lambda \end{cases} \tag{A.10}$$

By adopting an incompressible version of the hyperelastic Yeoh model for the uniaxial stress case, the following relation for the first Piola-Kirchhoff stress (force divided by initial area) can be obtained, see [1]:

$$\sigma_3 = \frac{P}{A} = 2\left(C_{10} + 2C_{20}\left(\frac{2}{\lambda} + \lambda^2 - 3\right) + 3C_{30}\left(\frac{2}{\lambda} + \lambda^2 - 3\right)^2\right)\left(\lambda - \frac{1}{\lambda^2}\right) \tag{A.11}$$

A.4 Fit to test data

To fit the Yeoh model to the experimental data, the following condition should be fulfilled to the greatest extent possible at each point:

$$\frac{S_i^{yeoh}}{S_i^{exp}} \approx 1 \tag{A.12}$$

where S_i^{yeoh} denotes the nominal stress obtained from equation (A.11) and S_i^{exp} the experimental data with the corresponding stretches λ_i. Inserting (A.11) in (A.12) for every experimental point yields an overdetermined linear equation system:

$$\mathbf{Ac} = \mathbf{b} \tag{A.13}$$

where the 3×1 matrix, $\mathbf{c}$, contains the sought-for constants C_{10}, C_{20}, C_{30}. For every solution, $\mathbf{c}^*$, of the system a residual can be determined:

$$\mathbf{e} = \mathbf{Ac}^* - \mathbf{b} \tag{A.14}$$

The solution that minimizes the residual is found by solving the following linear system of equations:

$$\mathbf{A^T A c} = \mathbf{A^T b} \tag{A.15}$$